

# From laterally modulated two-dimensional electron gas towards artificial graphene

L. Nádorník,<sup>1,2,\*</sup> M. Orlita,<sup>3,2,1</sup> N. A. Goncharuk,<sup>2</sup> L. Smrčka,<sup>2</sup> V. Novák,<sup>2</sup> V. Jurka,<sup>2</sup>  
K. Hruška,<sup>2</sup> Z. Výborný,<sup>2</sup> Z. R. Wasilewski,<sup>4</sup> M. Potemski,<sup>3</sup> and K. Výborný<sup>2,5</sup>

<sup>1</sup>*Faculty of Mathematics and Physics, Charles University, Ke Karlovu 3, 121 16 Praha 2, Czech republic*

<sup>2</sup>*Institute of Physics, ASCR, v.v.i., Cukrovarnická 10, 162 53 Praha 6, Czech Republic*

<sup>3</sup>*Laboratoire National des Champs Magnétiques Intenses,*

*CNRS-UJF-UPS-INSA, 25, avenue des Martyrs, 38042 Grenoble, France*

<sup>4</sup>*Institute for Microstructural Sciences, NRC, Ottawa, Ontario, Canada K1A 0R6*

<sup>5</sup>*Department of Physics, State University of New York at Buffalo, New York 142 60, USA*

(Dated: August 26, 2011)

We report on a measured non-linear in magnetic field dependence of cyclotron resonance absorption as well as its splitting into several modes in GaAs/Al<sub>x</sub>Ga<sub>1-x</sub>As heterostructures with an etched hexagonal lateral superlattice. Our explanation, based on the perturbation theory, describes the observed phenomena as a weak effect of the lateral potential on the two-dimensional electron gas. In parallel to experiments, we develop a simple theoretical model to calculate miniband structure of these hexagonally patterned two-dimensional structures and formulate four criteria that have to be satisfied to reach graphene-like physics in such systems, i.e., to prepare artificial graphene.

PACS numbers: 73.22.Pr, 73.21.Cd, 78.67.Pt

## I. INTRODUCTION

The range of approaches to explore Dirac fermions in condensed-matter physics has recently been extended beyond natural graphene<sup>1-3</sup> to artificially created lattices whose properties such as inter-site coupling or lattice constant can be tuned. One approach here is to subject gas of ultracold atoms to a honeycomb optical lattice<sup>4</sup> giving rise to Dirac cones in dispersion relations.<sup>5,6</sup> The same has been proposed for lithographically patterned two-dimensional electron gases (2DEGs) in semiconductor heterostructures<sup>7-9</sup> as shown in Fig. 1. Apart from studying the Dirac fermions on their own, an appealing perspective in such semiconductor-based systems would be to fabricate various proof-of-principle electronic devices originally proposed for natural graphene,<sup>10</sup> for instance filters and valves,<sup>11</sup> Veselago lenses,<sup>12</sup> or splitters.<sup>13</sup> The electron-beam lithography used to define the artificial honeycomb crystal potential, dubbed artificial graphene (AG),<sup>9</sup> allows for much easier control over the device details such as the edge geometry, additional or missing “atoms” than what would require an atom-by-atom manipulation in the case of natural graphene.

The subject of this paper, fabrication and theoretical description of AG, represents a special case of lateral semiconductor superlattices (SLs) intensively studied especially in the nineties. The body of widely explored phenomena can be roughly divided into two classes: classical and quantum-mechanical. Magneto-plasmons in far-infrared transmission<sup>14</sup> and commensurability oscillations<sup>15</sup> in a modulated 2DEG can be largely explained without invoking quantum mechanics.<sup>16,17</sup> On the other hand, SLs under strong magnetic fields, which leads to the magnetic breakdown,<sup>18</sup> as well as other more complex systems<sup>19,20</sup> require quantum-mechanical ingredients (Bohr-Sommerfeld quantization and tunneling between semiclassical orbits).

In this context, the Dirac cone in the AG spectrum is a delicate quantum-mechanical feature just as the Hofstadter butterfly<sup>21</sup> is, i.e., Landau bands emerging when  $p$  quanta of magnetic flux pierce  $q$  elementary cells of a square SL.<sup>22</sup> Despite promising recent progress,<sup>9,23,24</sup> a clear-cut evidence of Dirac fermions in AG has not yet been found. Most likely, such an evidence can be provided by magneto-transport and magneto-optical experiment by observing half-integer quantum Hall effect,<sup>1,2</sup> or by visualization of the unique  $\sqrt{B}$  scaling in the optical response due to inter-Landau level (inter-LL) transitions.<sup>25-27</sup> More careful engineering of AG struc-

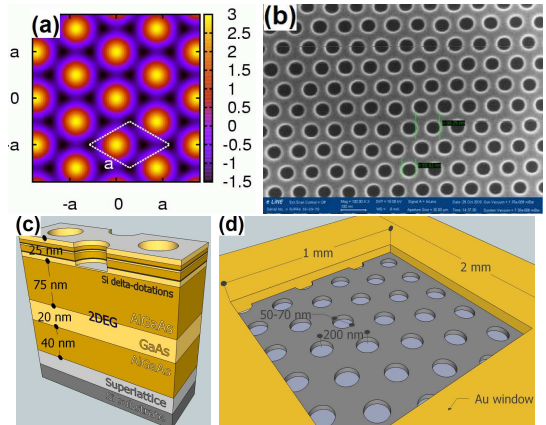


FIG. 1. (color online) Artificial graphene: Part (a): hexagonal potential of Eq. (1) defining the AG (in units of  $V_0$ ). Dark regions correspond to carbon atoms in the real graphene lattice; the primitive cell is indicated. (b): Scanning electron microscope image of the surface of one of the samples, (c): its atomic layer structure (2DEG depth  $\approx 100$  nm) and (d): the sample layout (not to scale).

tures is likely needed to realize these experiments.

In this paper, we explore the concept of artificial graphene both experimentally and theoretically. We use a simplified model of AG to formulate four straightforward criteria that must be fulfilled to achieve graphene-like physics in conventional 2D semiconductor heterostructures. Among them, the constraint on the lateral modulation potential strength has so far been assessed only indirectly<sup>23</sup> and we show how it can be inferred from infrared magneto-transmission experiments. We discuss necessary further steps needed to observe signatures of Dirac fermions in AG.

## II. THEORY

To arrive at transparent conditions necessary for the realization of Dirac fermions in the superlattice miniband structure, we use a maximally simplified AG model which is effectively single-parametric. The modulation potential  $V(\vec{r})$ ,  $\vec{r} = (x, y)$  shown at Fig. 1(a) is taken to comprise of three cosine functions

$$V(\vec{r}) = V_0(\cos \vec{g}_1 \vec{r} + \cos \vec{g}_2 \vec{r} + \cos \vec{g}_3 \vec{r}), \quad (1)$$

where  $\vec{g}_1 = 2\pi/a(1/\sqrt{3}, 1)$ ,  $\vec{g}_2 = 2\pi/a(2/\sqrt{3}, 0)$ ,  $\vec{g}_3 = \vec{g}_2 - \vec{g}_1$  are the basis-vectors of the graphene reciprocal space,  $a$  is the distance between two maxima of  $V(\vec{r})$  and  $V_0$  is the potential amplitude. Let us note that  $V_0$  has to be positive to obtain a potential of a honeycomb rather than a trigonal structure. If we construct the Hamiltonian matrix in basis  $\mathcal{B}$  of plane waves,

$$\mathcal{B} = \left\{ e^{i(\vec{k} + \vec{K}_{n_1 n_2})\vec{r}}, \vec{K}_{n_1 n_2} = n_1 \vec{g}_1 + n_2 \vec{g}_2 \right\}, \quad (2)$$

the ratio of diagonal to off-diagonal matrix elements is determined by  $V_0$  and  $a$ . Except for an overall scaling, the eigenvalues depend on a single dimensionless parameter

$$\zeta = \frac{m^*}{(2\pi\hbar)^2} V_0 a^2, \quad (3)$$

where  $m^*$  is the electron effective mass (in GaAs, 0.067 of the electron vacuum mass  $m_0$ ). Up to a factor of the order of unity, the parameter  $\zeta \simeq V_0/E_0$  is the ratio between strength of the modulation potential  $V_0$  and the kinetic energy  $E_0$  of a free electron at the  $K$  point of the Brillouin zone.

Depending on  $\zeta$ , we obtain miniband spectra that continuously vary from the free 2DEG, through nearly-free and more tight-binding-like models, up to nearly flat bands that correspond to practically isolated (artificial) atoms. This is illustrated in Fig. 2, where we plot miniband structure for four different values of  $\zeta$ . In Fig. 2a, we plot the parabolic dispersion of a free electron ( $\zeta = 0$ ) folded into the newly created Brillouin zone and then follow the evolution of the miniband structure with increasing  $\zeta$ , namely for  $\zeta = 0.3, 0.9$  and 4. The present

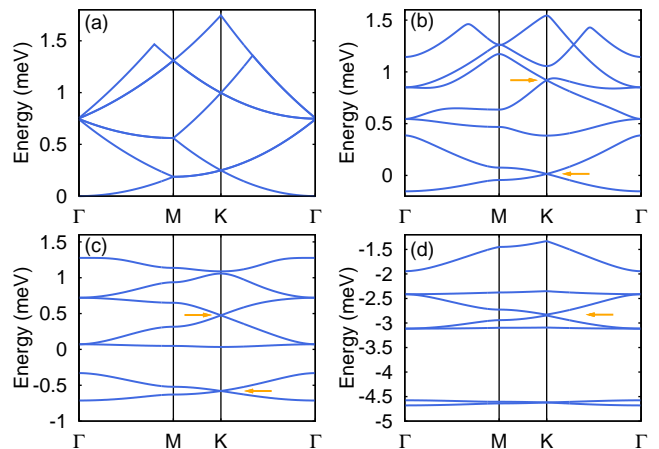


FIG. 2. (color online) Minibands generated for several values of the parameter  $\zeta$ . (a):  $\zeta = 0$ , dispersion of a free 2DEG. (b):  $\zeta = 0.3$ , first Dirac cone develops (indicated by arrow), the second one appears but remains covered by other bands. (c):  $\zeta = 0.9$ , both Dirac cones fully developed. (d):  $\zeta = 4.0$ , tight-binding type narrow minibands form and Dirac cones gradually flatten, ultimately becoming again unobservable. For  $a = 200$  nm, a,b,c, and d correspond to  $V_0 = 0, 0.4, 1$  and 4.5 meV in GaAs.

Dirac-cones are marked by vertical arrows and their pseudorelativistic character has been confirmed by analysing the corresponding wavefunctions.<sup>8</sup>

Importantly, more than one Dirac cone appears within the seven lowest lying minibands shown in Fig. 2. This fact, to the best of our knowledge so far not mentioned in literature, may significantly simplify the quest for pseudorelativistic physics as we discuss below. The Fermi velocity corresponding to the lower and upper Dirac cone for the modulation strength  $\zeta = 0.9$  (Fig. 2c) is roughly  $1.4 \times 10^4$  and  $3.6 \times 10^4$  m.s<sup>-1</sup>, respectively. The expected Fermi velocity in AG is thus more than order of magnitude lower as compared to natural graphene, where values around  $10^6$  m.s<sup>-1</sup> are reported.<sup>1</sup> Another important characteristics of the created Dirac cones is their width in energy  $E_{DC}$ . A closer inspection of Fig. 2 reveals that we always get the  $E_{DC}$  smaller than  $E_0$  and also that  $E_{DC}$  strongly depends on  $\zeta$ . In other words, the typical width of Dirac cones,  $E_{DC}$ , is dominantly given by two factors: the size of the Brillouin zone (i.e. the lattice constant  $a$ ) and the effective mass of the employed semiconductor system (which defines the kinetic energy  $E_0$ ).

Now we formulate four simple criteria which have to be fulfilled to achieve Dirac-like physics in hexagonally patterned heterostructures, i.e., to reach AG. Unless mentioned otherwise, we always consider lattice period  $a = 200$  nm and the effective mass of electrons in GaAs  $m = 0.067m_0$ , which match to the samples explored experimentally below.

(i) *Suitable miniband structure*: The effective strength of the modulation  $\zeta$  has to be tuned to get well-separated and well-developed Dirac cones. Consistently with our

calculations in Fig. 2, the range  $0.5 < \zeta < 4.0$  ensures that the Dirac cones do not overlap with other minibands, as is the case of low  $\zeta$  in Fig. 2b, and also the cones are not significantly flattened, which gradually happens for  $\zeta > 4$  towards the limit of isolated “atoms”. If we strictly limit ourselves to the upper Dirac cone, the effective strengths  $\zeta$  somewhat exceeding 4 are still acceptable. Let us note that the chosen range of  $\zeta$  corresponds to the potential modulation  $V_0$  that ranges from 0.6 to 4.5 meV.

(ii) *Fermi level positioning and/or carrier density*: The Fermi level has to be located in the vicinity of the developed Dirac cones. If these cones are well separated as required by the previous point, the corresponding carrier density is easy to estimate. The number of states in one miniband is equal to  $4/(\sqrt{3}a^2)$  with the spin degeneracy included. The carrier density then reaches  $n \approx 6 \times 10^9$  and  $2.5 \times 10^{10} \text{ cm}^{-2}$  with the Fermi level located at the Dirac point of the lower and upper cone, respectively. If we want to avoid experiments at extremely low densities (below  $10^{10} \text{ cm}^{-2}$ ), we should preferentially focus on the upper Dirac point. Another way, if technologically feasible, is to reduce the lattice constant. For instance, the lattice decreased to  $a = 100 \text{ nm}$  implies carrier densities that are four times higher. Notably, the miniband structure for such reduced lattice constant remains (after energy rescaling) the same as in Fig. 2(c).

(iii) *Low disorder*: The idealized miniband structure, as presented in Fig. 2, is in reality smeared out by disorder. The minimal requirement is to have the electron mean free path  $l_e = \hbar\mu\sqrt{2\pi n}/e^2$  significantly exceeding or at least comparable to the lattice constant  $a$ . For 2DEG with density of  $n = 10^{11} \text{ cm}^{-2}$  and the relatively low mobility  $\mu = 10^5 \text{ cm}^2/(\text{V.s})$ , the mean free path reaches  $l_e \approx 500 \text{ nm}$  and still remains well above the technologically achievable  $a$ .

(iv) *Careful probing*: A clear evidence for the presence of massless particles will likely come from experiments performed in magnetic fields, using transport<sup>1,2</sup> or optical<sup>25-27</sup> methods. Naturally, the characteristic spacing of LLs, given by the applied magnetic field  $B$  and by the effective Fermi velocity in AG, cannot exceed the Dirac cone width  $E_{DC}$ . Or optionally, the spacing of LLs in unpatterned 2DEG  $\hbar\omega_c \approx 2 \times B[\text{T}] \text{ meV}$  must be small in comparison to the modulation potential  $V_0$  and/or the width of the particular Dirac cone in AG,  $\hbar\omega_c \ll E_{DC}$ . Tolerable magnetic fields are thus hundreds of militesla, since the width of the Dirac cone reaches a few meV at most in technologically achievable structures. Such a low magnetic field requires high quality 2DEG samples. If we express this quality in terms of mobility, the accessible magnetic fields are then governed by a simple condition  $\mu B \gtrsim 1$ . In addition, it might be important to keep temperatures in sub-kelvin range ( $kT \ll \hbar\omega_c$ ) especially in magneto-transport experiments.

### III. EXPERIMENT

The lateral modulation of 2DEG is in most cases created either by gating using a specifically patterned metallic layer<sup>28,29</sup> or by etching the sample surface with a high spatial resolution.<sup>9,14,22,30,31</sup> In the more common latter case, arrays of dots or antidots are fabricated.<sup>32</sup> If we fix the spatial resolution of the chosen lithography technique, the antidots design allows us to get a slightly lower lattice constant of AG as compared to array of dots. The etching depth serves as a parameter tuning strength of the lateral potential. An especially strong modulation can be achieved by etching through the 2DEG layer. Such structures, with regions fully depleted from electrons,<sup>16</sup> have been mostly used to study magneto-plasmon effects.<sup>14</sup> On the other hand, quantum effects due to miniband structure are typically studied in shallow-etched samples;<sup>22</sup> we show below that this choice is indeed close to fulfil the first criterion of Sec. II.

The studied samples have been prepared by etching a relatively shallow array of holes (i.e. antidots) with a triangular symmetry. The electron beam lithography and dry etching process ( $\text{Ar}^+ + \text{SiCl}_4$ ) have been employed. We prepared three samples denoted as A, B and C, see Table I, with the etching depth of 15-25, 20 and 48 nm, respectively. The diameter of holes was always  $\approx 60 \text{ nm}$  and hole-to-hole distance, i.e., our AG lattice constant,  $a = 200 \text{ nm}$ . Samples A and B have been prepared from a wafer with 2DEG in a 20 nm-wide quantum well embedded between  $\text{Al}_{0.33}\text{Ga}_{0.67}\text{As}$  barriers and located 100 nm below the surface. The electrons in the well are provided by two  $\delta$ -doped Si layers, 15 nm ( $3 \times 10^{12} \text{ cm}^{-2}$ ) and 25 nm ( $2 \times 10^{12} \text{ cm}^{-2}$ ) deep, see Fig. 1(c). The sample C was fabricated from a simple  $\text{GaAs}/\text{Al}_{0.33}\text{Ga}_{0.67}\text{As}$  heterojunction located 115 nm below the sample surface. The triangular well formed at the interface was filled by electrons from a Si-doped  $\text{Al}_{0.33}\text{Ga}_{0.67}\text{As}$  region ( $1.5 \times 10^{18} \text{ cm}^{-3}$ ) separated from the interface by a spacer 25 nm wide. At all three samples, the lithographically patterned area ( $1 \times 1 \text{ mm}^2$ ) was surrounded by a gold frame (thickness 50 nm) to define the optically active part for the transmission experiment, see Fig. 1(d).

The prepared samples have been studied using the infrared magneto-spectroscopy technique, in this case having a form of the Landau level spectroscopy. To measure the magneto-transmission of the sample, the radiation of globar or mercury lamp was modulated by a Fourier transform spectrometer. We have used resolution down to 0.125 meV and worked at photon energies down to 4 meV. Afterwards, the radiation was delivered via light-pipe optics to the sample kept at 2 K inside a superconducting coil and detected by a Si bolometer, placed directly below the sample. All measurements were performed in the Faraday configuration with the magnetic field applied perpendicular to the sample layer.

The magneto-transmission experiment has been performed on all three prepared samples and the characteristic results are presented in Fig. 3. We plot there

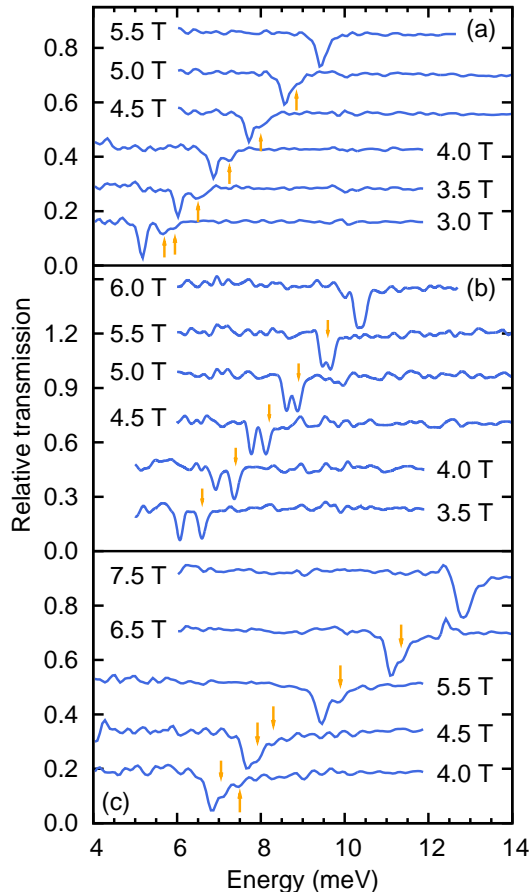


FIG. 3. (color online) Relative magneto-transmission spectra of studied samples A ( $d_{\text{holes}} \approx 15 - 25$  nm,  $d_{2\text{DEG}} = 100$  nm), B ( $d_{\text{holes}} = 20$  nm,  $d_{2\text{DEG}} = 100$  nm) and C ( $d_{\text{holes}} = 48$  nm,  $d_{2\text{DEG}} = 115$  nm) in parts (a), (b) and (c), respectively. The multi-mode character of cyclotron resonance absorption vanishes with the increasing magnetic field at  $B \approx 5, 6$  and  $7$  T in the sample A, B and C, respectively. All spectra are shifted vertically for clarity.

relative magneto-transmission spectra, i.e. transmission spectra at a given field normalized with respect to the response at  $B = 0$  T. A well-defined CR absorption of a nearly Lorentzian shape is obtained for all three samples at higher magnetic fields. When the magnetic field is lowered, we observe a more complex behavior with the CR absorption split into two or even more modes. The energy distance between these modes is clearly different in various samples and is positively correlated with the depth of the etched holes, i.e., with the strength of the modulation potential induced by the lateral patterning. An unpatterned reference sample, taken from the wafer used for fabrication of the samples A and B, has been also tested. As expected, it showed a typical Lorentzian-shaped CR absorption at the energy of  $\hbar\omega_c$  in the whole available range of magnetic fields.

Since the initial carrier concentration at dark was or

could be modified during technological processing and also, since the carrier concentration is affected by the near infrared part of the global/mercury lamp radiation (due to persistent photoconductivity), we estimated the carrier densities directly from the strength of cyclotron resonance.<sup>33</sup> This estimate has been done at higher fields, when all specimens provide a well-defined CR absorption of Lorentzian shape. The evaluated densities for the sample A, B and C are  $n_{A,B} \sim 0.7 \times 10^{11} \text{ cm}^{-2}$  and  $n_C \sim 1.8 \times 10^{11} \text{ cm}^{-2}$ , respectively. Optionally, this density could be further increased by illumination by an infrared diode. Using the CR absorption width, we roughly estimated also the carrier mobility in samples after processing which was found to be somewhat in excess of  $10^5 \text{ cm}^2/(\text{V}\cdot\text{s})$  for all three specimens.

#### IV. INTERPRETATION

We discuss two possible scenarios to interpret our experimental data. The first one relies on a quantum-mechanical (single-particle) approach and assumes the AG miniband structure due to the lateral periodic potential. These minibands are transformed into dispersively broadened LLs at non-zero magnetic field. The second scenario, a classical one, recalls characteristic multimode CR absorption observed in systems dominated by (confined) magneto-plasmons. We will show that this latter scenario is, if considered in detail, inconsistent with our measurements.

Now we summarize all the experimental facts and discuss them with respect to the four criteria to observe massless Dirac fermions in a laterally modulated 2DEG. This provides us with basic estimates on how close or far we are from Dirac-like conditions. These criteria, formulated in Sec. II, are related to the (mini)band electronic structure, carrier density, disorder in the system and also to the chosen experimental technique and conditions.

The observed departure from a single-mode CR mode at energy  $\hbar\omega_c$  shows a clear effect of the lateral modulation. Nevertheless, a deeper analysis, which follows later on, is required to give a reliable quantitative estimate for the potential amplitude  $V_0$  crucial for our first criterion about the suitable band structure. The carrier density, judged with respect to the used lattice constant  $a$ , is more than order of magnitude higher to reach the lowest Dirac cone. Even if we focus on the second Dirac cone, the density still remains too high, roughly three times. Slightly better situation is with the criterion related to the sample quality. The achieved mobility around  $\mu \sim 10^5 \text{ cm}^2/(\text{V}\cdot\text{s})$  corresponds to the mean free path  $l_e \sim 500$  nm which is above the lattice constant  $200$  nm, but further improvement of technology is still desirable to reach  $l_e \gg a$ . This carrier mobility would allow for meaningful experiments down to fields of few hundred of mT (fulfilling  $\mu B \gtrsim 1$ ) as required by the criterion on careful probing. Nevertheless, such low-field experiments (performed in THz spectral range) would

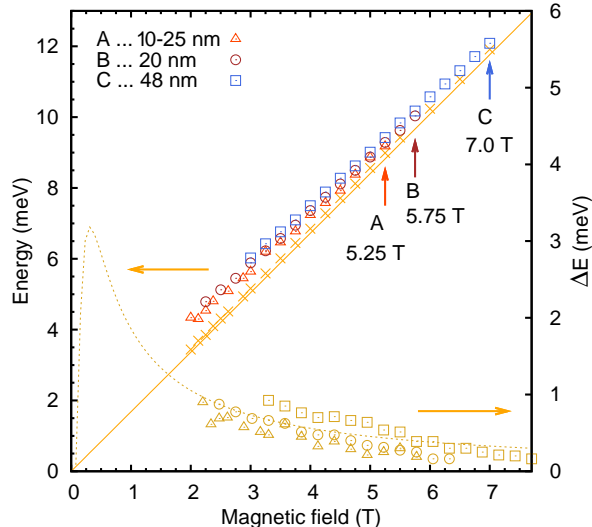


FIG. 4. (color online) Transitions observed in specimens A, B and C, cf. Fig. 3 (left vertical axis; depth of etched holes are indicated). Vertical arrows indicate magnetic fields at which the multi-mode character of CR absorption vanishes. The position of the main CR peak in spectra taken on the sample A is marked by crosses. The straight line corresponds to the theoretical CR-line position with an effective mass of  $m^* = 0.067m_0$ , which has been derived from measurements on reference (unpatterned) sample (not shown). Lower part of the figure (right vertical axis) shows determined values of the CR-line splitting  $\Delta E$ . The dashed line corresponds to the fit of  $\Delta E$  for the sample A based on the theoretical model discussed in the text.

only make sense at specimens with a significantly lower carrier density, i.e., with the Fermi level close to one of the Dirac points in AG band structure. It is just the interplay of the carrier density, technologically feasible lattice constant and a reasonably high mobility that will be crucial to deal with in the future preparation of AG.

We will now continue with a detailed analysis of our data to obtain quantitative estimates for the potential modulation  $V_0$  and show that infrared magneto-spectroscopy is a method suitable for this purpose. We start by noticing that the main absorption features in Fig. 3 still occur close to  $\hbar\omega_c$  but in contrast to the cyclotron resonance of an unmodulated 2DEG, they have an internal structure which disappears roughly as  $1/B$  (see Fig. 4) in the limit of high magnetic fields. Such behavior is suggestive of a perturbative effect from a potential whose strength becomes gradually weaker relative to the spacing of LLs. This spacing, the cyclotron energy  $\hbar\omega_c$ , then provides the dominant energy scale compared to the modulation potential  $V_0$  so that the small parameter  $V_0/\hbar\omega_c \propto 1/B$ . In the first-order perturbation calculation,<sup>34</sup> the unperturbed energies  $E_n =$

$\hbar\omega_c(n + 1/2)$  become broadened into bands:

$$E_{n,\kappa_x,\kappa_y} = E_n + V_0 e^{-2\beta^2/3} L_n(4\beta^2/3) \times \left\{ 2 \cos \beta^2(\kappa_x + \frac{1}{\sqrt{3}}) \cos \frac{\beta^2 \kappa_y}{\sqrt{3}} + \cos \frac{2\beta^2 \kappa_y}{\sqrt{3}} \right\} \quad (4)$$

where  $\beta^2 = 2\pi^2 \ell_0^2/a^2$ ,  $\ell_0^2 = \hbar/eB$  and  $\vec{\kappa}$  belongs to the hexagonal first magnetic Brillouin zone. Owing to special properties of Laguerre polynomials  $L_n$ ,<sup>35</sup> optical transition energies, that are  $E_{n+1,\kappa_x,\kappa_y} - E_{n,\kappa_x,\kappa_y}$ , can be rewritten in a simple way. Since we deal with low carrier concentrations at which only the lowest LL is occupied, we can restrain ourselves to  $n = 0$ ,

$$\Delta E_{1,0} = E_{1,\kappa_x,\kappa_y} - E_{0,\kappa_x,\kappa_y} = \hbar\omega_c - \frac{4}{3} V_0 \beta^2 e^{-2\beta^2/3} b(\kappa_x, \kappa_y) \quad (5)$$

where  $b(\kappa_x, \kappa_y)$  denotes the curled bracket of Eq. (4).

The optical transition energy  $\Delta E_{1,0}$  enters the absorption probability  $\alpha_{1,0}$  for a photon of frequency  $\omega$  that has caused transition between  $n = 0$  and  $n = 1$  LLs. Provided that the former (latter) LL is full (empty), this probability is proportional to

$$\int \frac{d^2 \kappa}{(2\pi)^2} |(1, \kappa_x, \kappa_y | p_x | 0, \kappa_x, \kappa_y)|^2 \delta(\Delta E_{1,0} - \hbar\omega). \quad (6)$$

If we neglect the dipole transition matrix element (transition between the mentioned two LLs is allowed by selection rules), the characteristic spectral features correspond to the van Hove singularities indicated in Fig. 5, in the occupation-weighted joint density of states (jDOS):

$$a(\omega) = \int \frac{d^2 \kappa}{(2\pi)^2} \delta(\Delta E_{1,0} - \hbar\omega) f_{0,\kappa_x,\kappa_y} (1 - f_{1,\kappa_x,\kappa_y}),$$

in which all those transitions at a given energy  $\hbar\omega = \Delta E_{1,0}$  count where the initial ( $n = 0$ ) state is occupied and the final ( $n = 1$ ) state is empty, as expressed by the Fermi-Dirac factors  $f$ . At a filling factor  $\nu = nh/eB = 2$ , which was assumed in expression (6),  $a(\omega)$  is a band of the width

$$w(B) = 6V_0 \beta^2 e^{-2\beta^2/3} \quad (7)$$

situated close to  $\omega = \omega_c$ . The width of the band decreases with decreasing  $\nu$  (at constant  $\beta$ ), as the filling of the  $n = 0$  LL decreases and smaller portions of the magnetic Brillouin zone become available for transitions. In the limit of very large  $B$ ,  $a(\omega)$  turns into a delta-peak at exactly  $\omega = \omega_c$ .

Eq. (7) provides a reasonable basis for interpretation of experimental data presented in Figs. 3(a)-(c). The peak-to-peak distance shown as the lower data sets in Fig. 4 follows the magnetic field dependence of  $w(B)$  allowing to extract the values of  $V_0$  for the particular sample. It should be noted however, that the peak splitting observed in experiments does not correspond to the full width  $w$  as calculated using Eq. (7) because the lower edge of the absorption band is suppressed for  $\nu < 2$ . This is the case

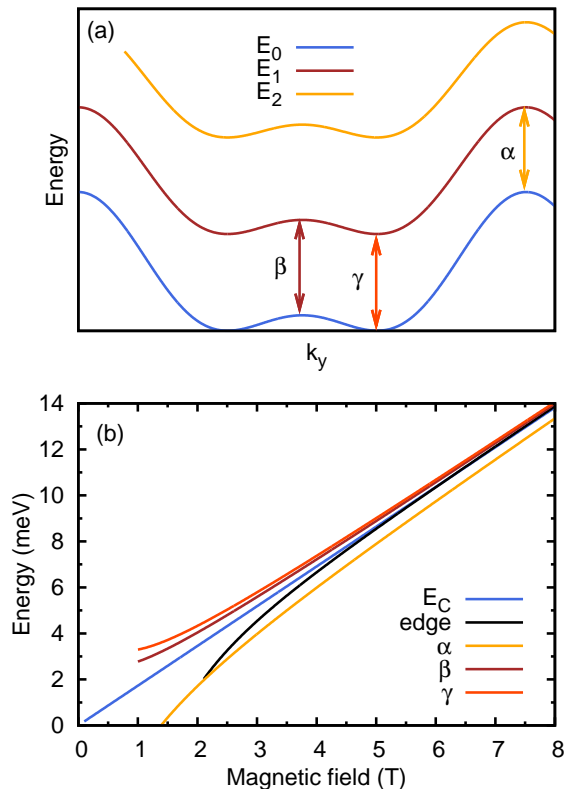


FIG. 5. (color online) Part (a): Schematic plot of three lowest lying LLs broadened into bands due to the lateral hexagonal modulation. Transitions related to the van Hove singularities in the joint density of states  $a(\omega)$  are marked by  $\alpha, \beta$  and  $\gamma$ . Whereas  $\alpha$  and  $\gamma$  are the band edges,  $\beta$  is the logarithmic singularity corresponding to the saddle point between two neighbouring minima of  $\Delta E_{10}$  in  $\vec{k}$ -space. Part (b): Magnetic field dependence of jDOS  $\alpha, \beta, \gamma$  singularity positions. “Edge” shows the lowest in energy allowed transition, as defined by the position of the Fermi level (for  $n = 1.0 \times 10^{11} \text{ cm}^{-2}$ ).  $E_c = \hbar\omega_c$  is the cyclotron energy.

Sample	$d_{\text{holes}}$	$d_{2\text{DEG}}$	$V_0$	$\zeta$
A	15-25	100	2.2 meV	2.4
B	20	100	3.5 meV	3.1
C	48	115	4 meV	3.6

TABLE I. Potential amplitude  $V_0$  and the corresponding dimensionless parameter  $\zeta$  for samples A, B and C as derived by fitting our data using Eq. (7), see text for details. The etching depths and the distances from 2DEG to the sample surface are also listed.

of  $B > 2 \text{ T}$  and  $n < 10^{11} \text{ cm}^{-2}$  when spin degeneracy remains unresolved; we note that the Zeeman splitting  $\varepsilon_z$  is roughly  $50\times$  smaller than the LL broadening at  $B = 2 \text{ T}$ ,  $\varepsilon_z = g\hbar/2m_0B \approx 0.05 \text{ meV}$ . Features of the jDOS appearing in the absorption band scale as  $cw(B)$ , where  $0 < c < 1$  is a constant. These features are shown in Fig. 5 and correspond to the indicated transitions of the broadened Landau bands  $E_{n,\kappa_x,\kappa_y}$ . The first states

that become depopulated upon the filling factor dropping below two (that is when the magnetic field is increased) are those close to the top of the band. Correspondingly, the transitions  $\alpha$  are the first ones to disappear from the absorption spectra.

For the remaining two features  $\beta$  and  $\gamma$ , our form of the potential  $V(x, y)$  would imply  $c = 1/9$ . However, since the transition  $\beta$  gives rise to a logarithmic singularity which is likely to be smeared out, we focus on another candidate for an absorption feature: the Fermi edge which is also shown in the lower panel of Fig. 5 (transitions from the states close to  $E_F$  to the next Landau band). Although the Fermi edge does not precisely scale with  $w(B)$ , it appears at frequencies  $\omega \approx \omega_c$  hence we take  $c \approx 1/3$ . The values of  $V_0$  inferred from fitting our data, assuming that the splitting of the CR mode corresponds to  $\frac{1}{3}w(B)$ , are shown in Tab. I alongside with the corresponding  $\zeta$ . These values confirm, as anticipated at the beginning of Sec. III, that shallow etching may create modulation potential favorable for Dirac-fermion physics in AG as quantified by the first criterion in Sec. II.

As mentioned above, the splitting of the cyclotron resonance absorption in diminishing magnetic fields, as shown in Fig. 3, can also be reminiscent of magneto-plasma oscillations in 2DEG.<sup>36</sup> Indeed, the magneto-optical response of our samples, which consists from a basic CR absorption line accompanied by one or more modes at (only) higher energies, resembles spectra taken on 2DEG with 1D lateral modulation (stripe geometry) or on an unmodulated 2DEG, but under 1D finite-size effects.<sup>37–39</sup> Nevertheless, a more relevant comparison is one to the response of magneto-plasmons in a 2DEG subject to lateral modulation in both directions, in particular in antidot lattices.<sup>14,40</sup> In such a case, the far infrared or microwave magneto-absorption response includes, among others, a characteristic lower branch located below the CR energy, which is well documented experimentally and explained theoretically. This lower branch is interpreted as an edge-magneto-plasmon (EMP), circulating around the antidot, and its existence is not directly connected with the symmetry of the antidot lattice.<sup>16,41</sup>

No sign of any EMP mode below CR energy has been observed in our data, hence barring us from interpreting the observed multi-mode CR response in terms of magneto-plasmons. It should also be noted here that magneto-plasmon behavior has been detected experimentally only at significantly higher densities.<sup>14,40</sup> Independently of these considerations, we also performed another test to exclude magneto-plasmon effects. We used external illumination by an infrared diode to gradually increase the carrier density  $n$  in the sample B (as evidenced by the strength of the CR absorption at high magnetic fields). The distance of observed modes shown in Fig. 6 decreased rather than increased with  $n$ , which is the opposite trend than expected from plasmons.

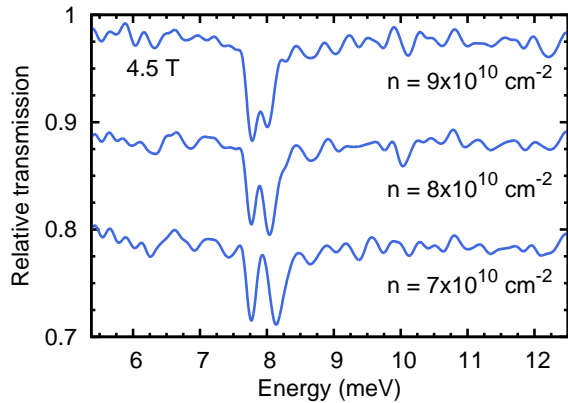


FIG. 6. (color online) Magneto-transmission spectra (shifted vertically for clarity) taken on the sample B at  $B = 4.5$  T with three different carrier concentrations adjusted by gradually increased illumination time. Splitting of the observed modes clearly decreases with increasing carrier density.

## SUMMARY AND CONCLUSIONS

The concept of artificial graphene has been explored both experimentally and theoretically. Based on a simple theoretical model, we formulated four basic criteria that need to be met in order to create and experimentally demonstrate the proposed graphene-like bands in modulated semiconductor heterostructures. We have prepared three samples with lateral modulation and investigated them using infrared magneto-spectroscopy. The results have been discussed with respect to the proposed criteria with the following conclusions. Etching an antidot (hole) lattice on the sample surface creates lateral modulation potential with favorable strength, i.e., one that gives rise to a miniband structure containing well-developed Dirac cones. An empirical rule, which connects the depth of etched holes with the strength of the lateral potential,

has been found for the specified technological protocol. The quality of prepared specimens, expressed in terms of mobility or mean free path, has been evaluated as sufficient to resolve the AG electronic structure with the Dirac cones, nevertheless, further increase of this quality would be desirable. The main obstacle, preventing up to now realization of Dirac-like physics in 2DEG, seems to be related to the interplay between the electron density and the lattice constant. Since lowering carrier density down to  $10^9$   $\text{cm}^{-2}$  range seems unrealistic, we instead logically suggest to reduce the lattice constant below 100 nm. This is technologically challenging, given the constraints on mobility, nevertheless still feasible. Furthermore, we propose to focus on a higher Dirac cone, which is found in AG miniband structure and which could be probed at higher carrier densities, namely at  $n \approx 10^{11}$   $\text{cm}^{-2}$  for  $a = 100$  nm. With these suggestions, we believe that massless Dirac fermions can be observed in laterally modulated 2DEG, probably using infrared or THz magneto-spectroscopy or magneto-transport technique, in (possibly not too distant) future.

## ACKNOWLEDGEMENTS

The authors would like to sincerely thank P. Hubík and J. Čermák for technological assistance and J. Wunderlich for valuable critical remarks. Moreover, the support of the following institutions is acknowledged: the Ministry of Education of the Czech Republic projects LC510 and MSM0021620834, GAUK No. 425111, GACR No. P204/10/1020, the Academy of Sciences of the Czech Republic via Institutional Research Plan No. AV0Z10100521, GAAV contract KJB100100802, Foundation *NanoScience* via project Dispograph and Præmium Academiæ and last but not least, EC-EuroMagNetII under Contract No. 228043.

\* nadvl@fzu.cz

<sup>1</sup> K. S. Novoselov, A. K. Geim, S. V. Morozov, D. Jiang, M. I. Katsnelson, I. V. Grigorieva, S. V. Dubonos, and A. A. Firsov, *Nature* **438**, 197 (2005).

<sup>2</sup> Y. B. Zhang, Y. W. Tan, H. L. Stormer, and P. Kim, *Nature* **438**, 201 (2005).

<sup>3</sup> A. K. Geim and K. S. Novoselov, *Nature Mater.* **6**, 183 (2007).

<sup>4</sup> G. Grynberg, B. Lounis, P. Verkerk, J.-Y. Courtois, and C. Salomon, *Phys. Rev. Lett.* **70**, 2249 (1993).

<sup>5</sup> S.-L. Zhu, B. Wang, and L.-M. Duan, *Phys. Rev. Lett.* **98**, 260402 (2007).

<sup>6</sup> B. Wunsch, F. Guinea, and F. Sols, *New Journal of Physics* **10**, 103027 (2008).

<sup>7</sup> C.-H. Park, L. Yang, Y.-W. Son, M. L. Cohen, and S. G. Louie, *Phys. Rev. Lett.* **101**, 126804 (2008).

<sup>8</sup> C.-H. Park and S. G. Louie, *Nano Letters* **9**, 1793 (2009).

<sup>9</sup> M. Gibertini, A. Singha, V. Pellegrini, M. Polini, G. Vignale, A. Pinczuk, L. N. Pfeiffer, and K. W. West, *Phys. Rev. B* **79**, 241406 (2009).

<sup>10</sup> Dubois, S. M.-M., Zanolli, Z., Declerck, X., and Charlier, J.-C., *Eur. Phys. J. B* **72**, 1 (2009).

<sup>11</sup> A. Rycerz, J. Tworzydło, and C. W. J. Beenakker, *Nature Phys.* **3**, 172 (2007).

<sup>12</sup> V. V. Cheianov, V. Fal'ko, and B. L. Altshuler, *Science* **315**, 1252 (2007).

<sup>13</sup> J. L. Garcia-Pomar, A. Cortijo, and M. Nieto-Vesperinas, *Phys. Rev. Lett.* **100**, 236801 (2008).

<sup>14</sup> K. Kern, D. Heitmann, P. Grambow, Y. H. Zhang, and K. Ploog, *Phys. Rev. Lett.* **66**, 1618 (1991).

<sup>15</sup> D. Weiss, K. V. Klitzing, K. Ploog, and G. Weimann, *EPL (Europhysics Letters)* **8**, 179 (1989).

<sup>16</sup> S. A. Mikhailov, *Phys. Rev. B* **54**, R14293 (1996).

<sup>17</sup> C. W. J. Beenakker, *Phys. Rev. Lett.* **62**, 2020 (1989).

- <sup>18</sup> P. Středa and A. H. MacDonald, *Phys. Rev. B* **41**, 11892 (1990).
- <sup>19</sup> C. Albrecht, J. H. Smet, D. Weiss, K. von Klitzing, R. Henning, M. Langenbuch, M. Suhrke, U. Rössler, V. Umansky, and H. Schweizer, *Phys. Rev. Lett.* **83**, 2234 (1999).
- <sup>20</sup> S. Olszewski, M. Pietrachowicz, and M. Baszczak, *phys. stat. sol. (b)* **241**, 3572 (2004).
- <sup>21</sup> D. R. Hofstadter, *Phys. Rev. B* **14**, 2239 (1976).
- <sup>22</sup> M. C. Geisler, J. H. Smet, V. Umansky, K. von Klitzing, B. Naundorf, R. Ketzmerick, and H. Schweizer, *Phys. Rev. Lett.* **92**, 256801 (2004).
- <sup>23</sup> G. De Simoni, A. Singha, M. Gibertini, B. Karmakar, M. Polini, V. Piazza, L. N. Pfeiffer, K. W. West, F. Beltram, and V. Pellegrini, *Appl. Phys. Lett.* **97**, 132113 (2010).
- <sup>24</sup> A. Singha, M. Gibertini, B. Karmakar, S. Yuan, M. Polini, G. Vignale, M. I. Katsnelson, A. Pinczuk, L. N. Pfeiffer, K. W. West, and V. Pellegrini, *Science* **332**, 1176 (2011).
- <sup>25</sup> M. L. Sadowski, G. Martinez, M. Potemski, C. Berger, and W. A. de Heer, *Phys. Rev. Lett.* **97**, 266405 (2006).
- <sup>26</sup> Z. Jiang, E. A. Henriksen, L. C. Tung, Y.-J. Wang, M. E. Schwartz, M. Y. Han, P. Kim, and H. L. Stormer, *Phys. Rev. Lett.* **98**, 197403 (2007).
- <sup>27</sup> R. S. Deacon, K.-C. Chuang, R. J. Nicholas, K. S. Novoselov, and A. K. Geim, *Phys. Rev. B* **76**, 081406 (2007).
- <sup>28</sup> A. Soibel, U. Meirav, D. Mahalu, and H. Shtrikman, *Semiconductor Science and Technology* **11**, 1756 (1996).
- <sup>29</sup> S. Hugger, T. Heinzl, and T. Thurn-Albrecht, *Appl. Phys. Lett.* **93**, 102110 (2008).
- <sup>30</sup> J. Takahara, A. Nomura, K. Gamo, S. Takaoka, K. Murase, and H. Ahmed, *Jap. J. of Appl. Phys.* **34**, 4325 (1995).
- <sup>31</sup> M. C. Geisler, S. Chowdhury, J. H. Smet, L. Höppel, V. Umansky, R. R. Gerhardts, and K. von Klitzing, *Phys. Rev. B* **72**, 045320 (2005).
- <sup>32</sup> D. Heitmann and J. P. Kotthaus, *Physics Today* **46**, 56 (1993).
- <sup>33</sup> K. Chiu, T. Lee, and J. Quinn, *Surface Science* **58**, 182 (1976).
- <sup>34</sup> X. F. Wang, P. Vasilopoulos, and F. M. Peeters, *Phys. Rev. B* **69**, 035331 (2004).
- <sup>35</sup> I. S. Gradshteyn and I. M. Ryzhik, “Table of integrals, series, and products,” (Academic, New York, 1980).
- <sup>36</sup> F. Stern, *Phys. Rev. Lett.* **18**, 546 (1967).
- <sup>37</sup> S. A. Mikhailov and N. A. Savostianova, *Phys. Rev. B* **71**, 035320 (2005).
- <sup>38</sup> S. A. Mikhailov and N. A. Savostianova, *Phys. Rev. B* **74**, 045325 (2006).
- <sup>39</sup> O. M. Fedorych, S. A. Studenikin, S. Moreau, M. Potemski, T. Saku, and Y. Hirayama, *Int. J. of Mod. Phys. B* **23**, 2698 (2009).
- <sup>40</sup> Y. Zhao, D. C. Tsui, M. Santos, M. Shayegan, R. A. Ghanbari, D. A. Antoniadis, and H. I. Smith, *Appl. Phys. Lett.* **60**, 1510 (1992).
- <sup>41</sup> S. A. Mikhailov and V. A. Volkov, *Phys. Rev. B* **52**, 17260 (1995).